# INFLUENCE OF THE LEAKAGE CURRENT ON THE PERFORMANCE OF LARGE AREA SILICON DRIFT DETECTORS.

Claudio Piemonte[1], Alexander Rashevsky[1], Denis Nouais[2]
[1)] *INFN, Sezione di Trieste, Via A. Valerio 2, I-34127 Trieste, Italy*
[2)] *INFN, Sezione di Torino, Via P. Giuria 1, I-10125 Torino, Italy*

**Abstract**

In this paper we investigate the influence of the leakage current on the performance of Silicon Drift Detectors. First, analytical considerations are given in order to highlight the problems, specific for this type of detector, that emerge with leakage current. Then the obtained results are compared with the data of laboratory measurements. Aiming at a mass production of SDDs for the Inner Tracking System of the ALICE experiment at LHC we propose a simple and fast measurement for a preliminary selection before passing to a detailed acceptance test.

## 1 Introduction

Starting from the first results of Gatti and Rehak [1]-[5], the SDD development has made a remarkable progress. Nevertheless the production, on a large scale and with a good yield, of detectors which satisfy the acceptance conditions imposed by an experiment is still a challenge. One of the conditions is a low leakage current in all the cathodes, because even one single defect manifested by high current can affect the whole detector. The Inner Tracking System (ITS) of the ALICE experiment at LHC will require a production of about $300$ silicon drift detectors [6]. Assuming that the final yield will not be of $100\%$ this number will be higher. Taking into account the complexity of SDDs, a full analysis of each one will require several hours. That is why it is quite important to perform some preliminary measurements of $(I - V)$ characteristics, both in single cathodes and in the detector as a whole, in order to preselect in a simple way the detectors coming from the mass production.

## 2 Basic SDD structures

The design of most of the linear SDDs [7]-[14] necessarily presents the following structures (Fig. 1): a series of parallel *drift cathodes* ($p^+$ implant strips in the case of *n*-type

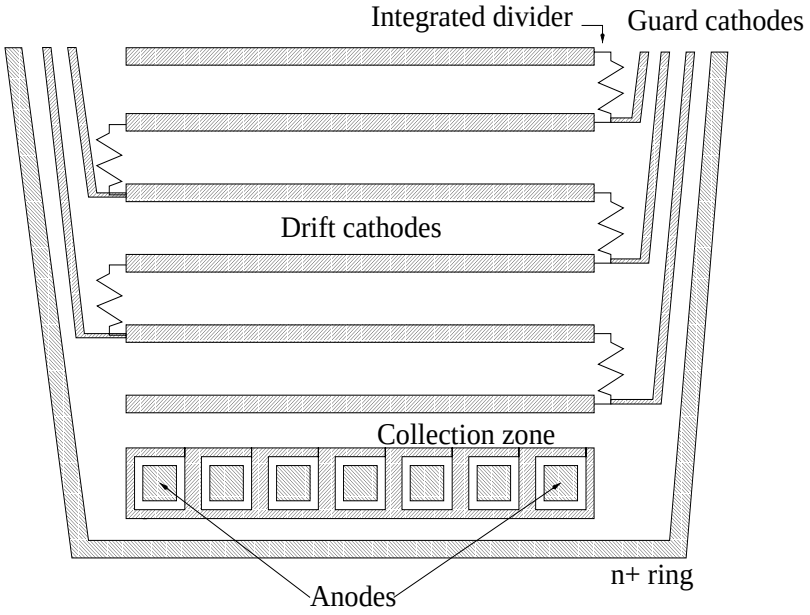


Figure 1: Basic SDD structures (*n*-side).

silicon substrate) forming a drift region is realized on both sides of the detector, both to

fully deplete its volume and to provide a constant electrostatic field parallel to the wafer surface. Drift cathodes are biased through a *high voltage divider*. In a large scale application of SDDs it is important to minimise the number of external connections to the detector, thus, it is very desirable to integrate the high voltage divider in the detector substrate. This can be done with high resistivity $p^+$ implants or polysilicon resistors. *Guard electrodes* connected with a certain periodicity to the drift cathodes serve to scale gradually the high potential of the drift area down to the ground potential of the $n^+$ ring at the detector edge. Usually, some of the drift cathodes closest to the anodes are externally biased and serve to bring drifting charges effectively from the middle plane of the detector towards the surface where they are collected by an array of $n^+$ anodes. Normally, this part of the drift region is referred to as the '*collection zone*'. Conventionally, the anode side of the SDD is called *n*-side (as only this side presents $n^+$ implants) and the other side is called *p*-side. The drift velocity in the SDD is very sensitive to temperature variations in the silicon substrate (about $1\%/K$) [15]. The current flowing in the integrated high voltage divider causes heat dissipation which gives rise to certain temperature gradients in the sensitive region of the SDD. That is why it is very important to have a way to monitor 'on-line' the drift velocity across the sensitive area in order to calibrate the drift time for temperature variations [16], [17]. This can be accomplished with a suitably designed structure of charge injectors (infrared laser, *n*-type implants or MOS capacitors).

## 3 Impact of the leakage current on the SDD performance.

Let's consider the leakage current constituted by the current due to possible local defects and by the dark current generated both in the depleted bulk and at the $Si-SiO_2$ interface. While in silicon microstrip or pixel detectors locally generated high current is confined within few strips/pixels, a similar defect in the SDD is propagated throughout the whole detector. Normally, a few percent of strip/pixels with high current are tolerated in the acceptance requirements for these detectors. This is not the case of the SDD, where a single local defect generating high current can make the whole detector unusable. The defects are manifested either as generation centres or as a premature breakdown. Generation centres can be situated both in the bulk and at the surface of the semiconductor, while breakdown occurs in the vicinity of p-n junction. When the defect is localised in the drift region of the SDD, the electron component of the current is collected at the end of the drift region by $n^+$ anodes and constitutes the '*hot spot*' on the anode array (Fig. 2). Due to diffusion and electrostatic repulsion the '*hot spot*' has a gaussian-like shape. The hole component is collected by the nearest drift cathodes.

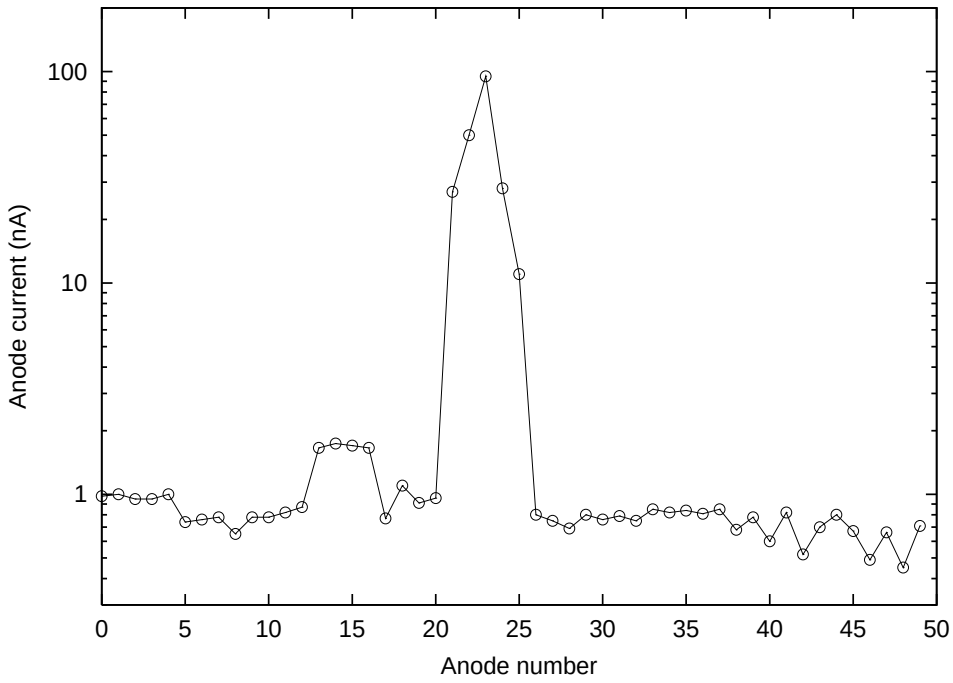


Figure 2: Anode current distribution with a 'hot spot'.

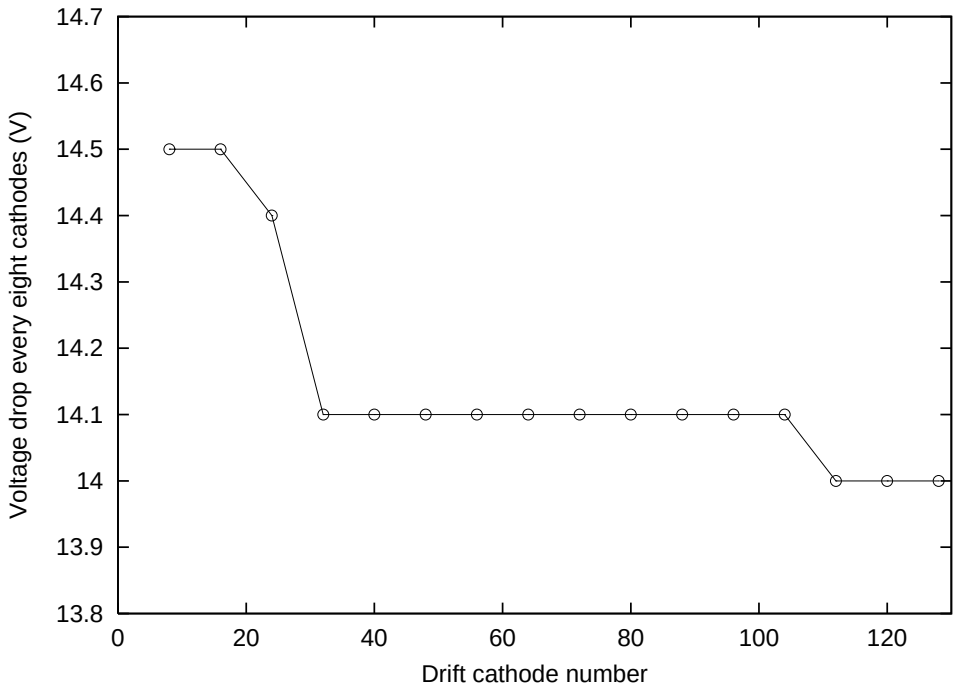


Figure 3: Potential drop between eight consecutive drift cathodes as a function of drift cathode number. The step of $0.4V$ corresponds to the *hot-spot* shown in figure 2.

If the defect is localised in the bulk close to the middle plane of the detector, the hole current will be distributed between the drift cathodes of both sides. When the defect is found in the detector part occupied by the guard cathodes, the electron current drifts towards the detector edge reaching the $n^+$ ring surrounding the detector, while the hole current is collected by the guard strips. Entering the cathode chain of the SDD constituted by the drift cathodes, high voltage divider and guard cathodes, the hole current is added to the high voltage divider current and can alter the potential distribution on the drift cathodes (Fig. 3). Since a linear potential distribution is mandatory to maintain the drift field constant (for an easy reconstruction of the impact point in the drift direction), one should choose carefully the value of the implanted resistors. On one hand, this value should not be too low as it leads to excessive heat dissipation and temperature gradients in the drift region. On the other hand, the current flowing through the cathode chain should be high enough in comparison with the hole leakage current, at least in absence of local defects generating high current.

To give a quantitative analysis of the leakage current impact on the SDD performance let's consider the large area prototype produced by Canberra Semiconductors N.V., Belgium, for the ALICE ITS. This detector is realized on NTD (Neutron Transmutation Doped) $5''$ silicon wafers with a resistivity of $3000\Omega \cdot cm$ and a thickness of $300\mu m$. It is a bi-directional structure. For each half detector the drift length is $35.0mm$, the drifting charge is collected by $256$ anodes with a pitch of $294\mu m$, so that the sensitive area is $75.3mm$ wide. The sensitive-to-total area ratio is $88\%$. The divider is integrated on the detector and the resistor connecting two consecutive drift cathodes has the value of $170k\Omega$.

There are two requirements regarding the leakage current.

One is related to the design of the front-end electronics. The preamplifier input is directly coupled to the anodes, but, since the design allows for at least $500nA$ of input current before the dynamic range starts to be affected, only the noise implications of the anode leakage current need to be considered. The normal noise should not be more than $250$ electrons for a single channel [6]. We choose an upper limit of $300$ electrons above which the efficiency of that channel is considered compromised. The simulated response function of the preamplifier/shaper chip is very close to $RC-CR^2$, with a peaking time of $36ns$ and a noise performances of $150e^-$ + $22e^-/pF$. The following table gives the noise contribution due to the anode current calculated using the theoretical response function, and the total noise considering a load capacitance of $2pF$.

| **Anode current** (nA) | 0 | 1 | 10 | 20 | 50 | 100 | 200 | 500 |
|---|---|---|---|---|---|---|---|---|
| **Anode current noise** ($e^-$) | 0 | 18 | 56 | 79 | 125 | 177 | 250 | 395 |
| **Total noise** ($e^-$) | 194 | 195 | 202 | 209 | 231 | 262 | 316 | 440 |

A limit of $100nA$ for the anode current can be considered "safe" enough, taking into account the leakage current increase due to accumulated radiation dose.

The second requirement comes from a limit of $30\mu m$ on the position resolution along the drift direction [6]. As it was mentioned, the hole component of the leakage current entering the cathode chain alters the linearity of the potential distribution on the high voltage divider. This gives a systematic error on the position resolution along the drift direction. It is always possible to get rid of this error constructing the calibration curve for the detector. Obviously, it is quite onerous to perform this procedure for each of the $300$ SDDs needed for the ITS. For this reason it is desirable to include the systematic error due to the non-linearity of the detector in the position resolution limit. Presently we can not disentangle the various contributions to this limit. Arbitrarily we can decide that the systematic error component that we can afford is $21\mu m$. The other part is made up by the noise due to detector and electronics, temperature variation and the non-uniformity of the resistivity of silicon.

Now we demonstrate the influence that a single defect generating high current has on the linearity of the potential distribution on the integrated divider and, consequently, on the position resolution. The total number of drift cathodes is $292$, so at $U_{bias} = -2328V$ (the expected working bias voltage) the current flowing through the divider is $I_{div} = 2328V/(291 \cdot 170k\Omega) \simeq 47\mu A$. This ideal case is illustrated in figure 4a-b, where the

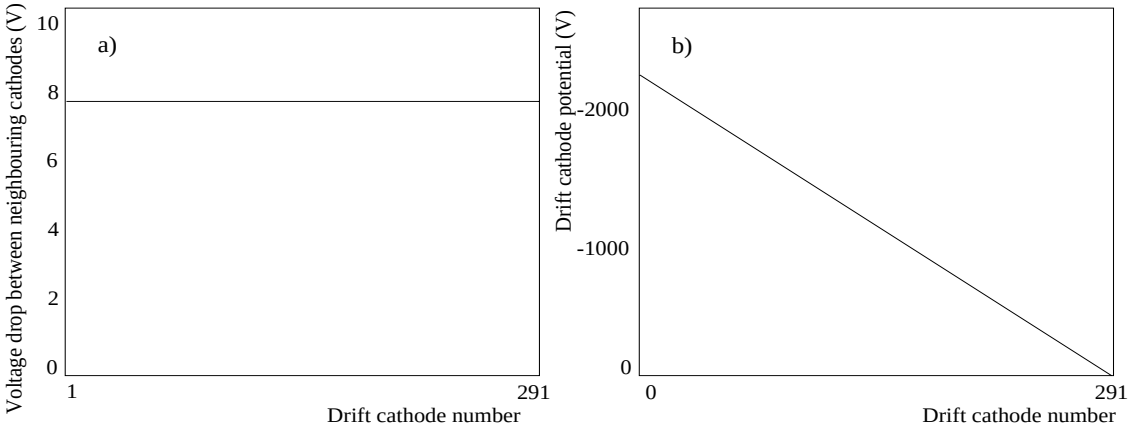


Figure 4: Voltage drop between consequent drift cathodes (a) and potential distribution on the divider (b) as a function of the drift cathode number.

voltage drop between neighbouring cathodes and the resulting potential on the divider are presented as a function of the drift cathode number. The potentials on the divider are referred to the potential of the last cathode connected to the divider, that is $-40V$. If there is a local defect close to the drift cathode $n$, a current $I_n$ enters the divider through this

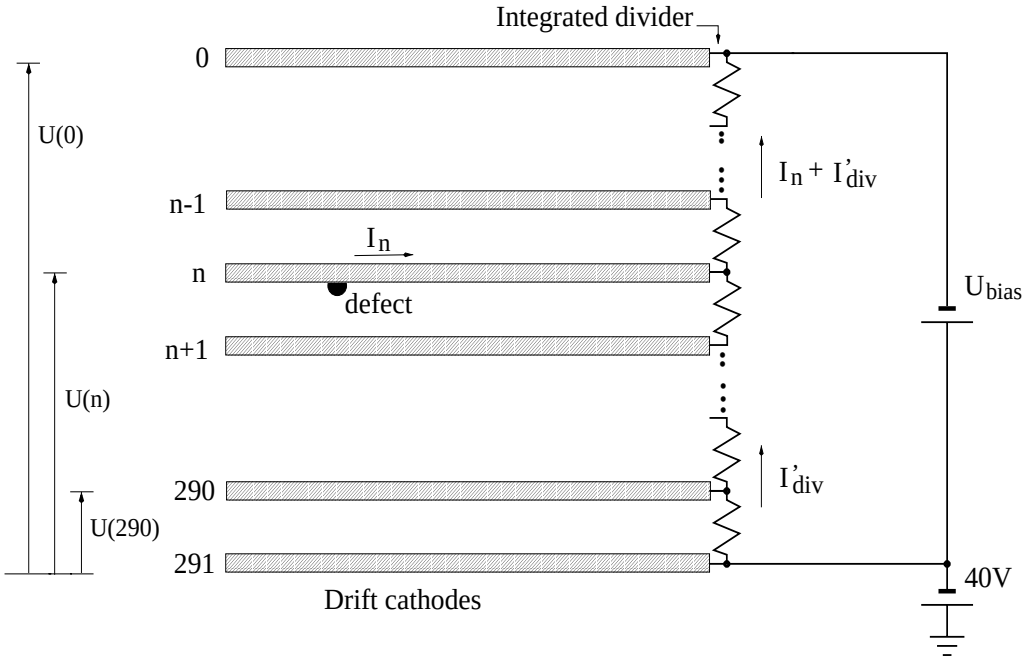


Figure 5: A defect on a cathode generates a current that enters the divider.

cathode (Fig. 5). In this situation

$$U_{bias} = 291 r I'_{div} + n r I_n, \tag{1}$$

so

$$I'_{div} = I_{div} - \frac{n}{291} I_n. \tag{2}$$

The potential on the cathode $k$ is described by the following equation:

$$U(k) = \begin{cases} (291-k) r I'_{div} + (n-k) r I_n & 0 \le k \le n \\ (291-k) r I'_{div} & n \le k \le 291 \end{cases} \tag{3}$$

Figure 6 illustrates the variation $\delta u$ of the potential drop between neighbouring drift cathodes *(a)* and the potential distribution *(b)* as a function of the defective cathode number. The variation $\delta u$ is:

$$\delta u = r(I_n + I'_{div}) - r I'_{div} = r I_n. \tag{4}$$

The resulting potential deviation from the ideal distribution reaches its maximum $\Delta U$ on the defective drift cathode $n$ (Fig. 7b). $\Delta U$ is given by:

$$\Delta U = n r (I_n + I'_{div}) - n r I_{div}. \tag{5}$$

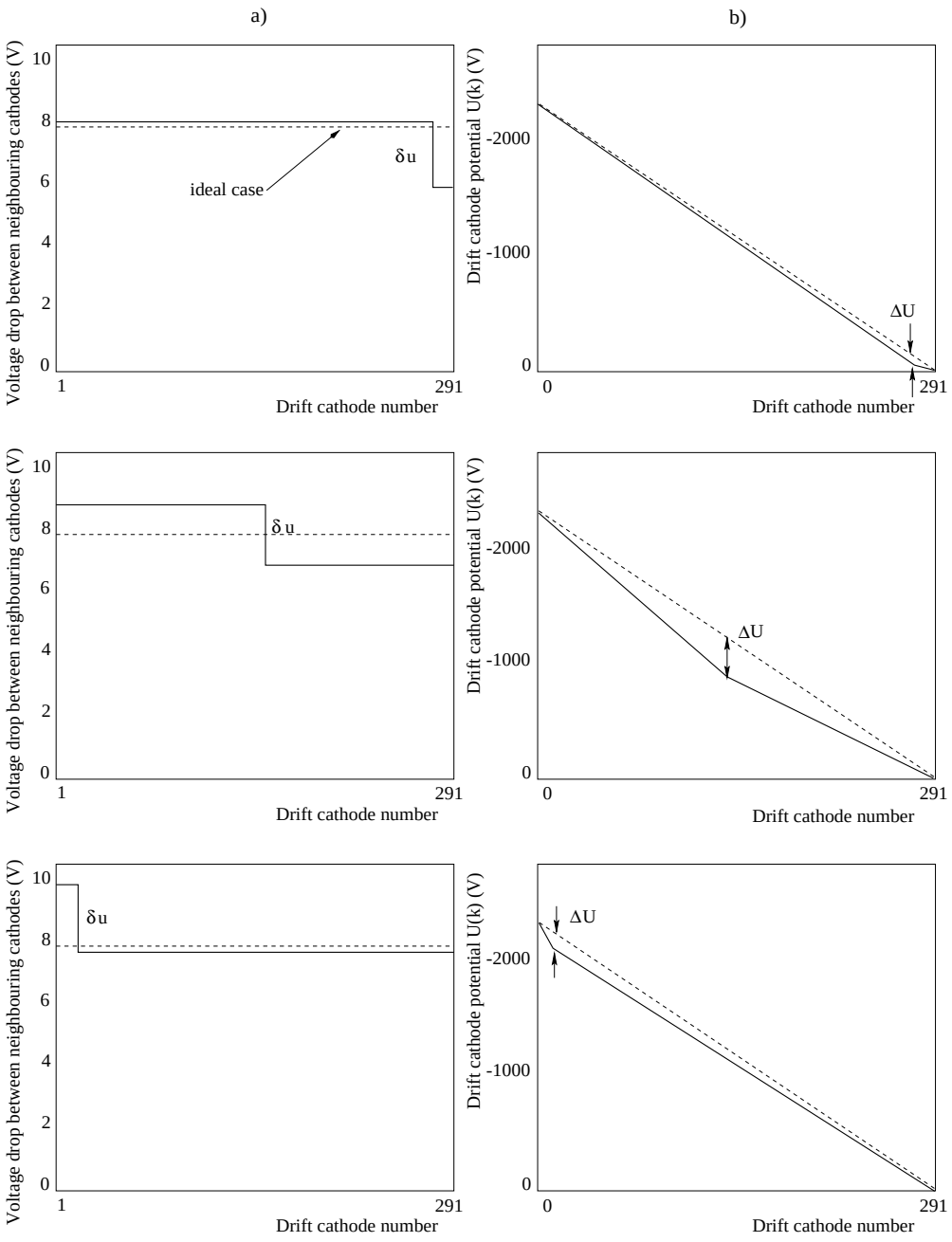


Figure 6: Potential distributions for three different positions of the defect in the drift region.

It is worthwhile noting that for the same current $I_n$ the value $\Delta U$ depends on the drift cathode number while $\delta u$ remains the same. We simulated the effect of a single local defect situated on one side of the detector for different values of $\delta u$. Figure 7 shows the deviation $\Delta U$ as a function of the defect location. The worst case is when the current $I_n$ enters the drift cathode in the middle of the drift region. In addition to the deterioration of

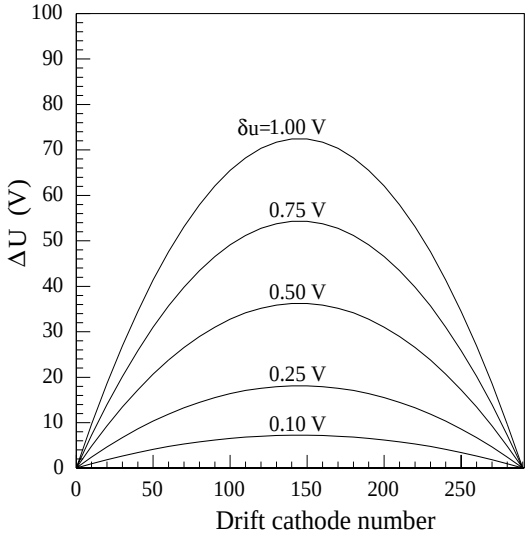


Figure 7: Maximum variation of the potential distribution on the divider from the ideal distribution as a function of the defect position.

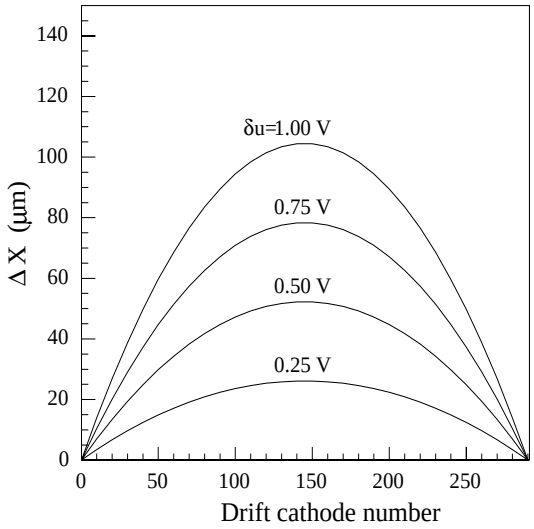


Figure 8: Maximum deviation of the bottom of the potential gutter from the middle of the wafer thickness as a function of the defect position.

the drift linearity there is also a shift of the bottom of the potential gutter from the middle of the wafer thickness. The shift reaches its maximum $\Delta X$ in front of the defective drift cathode. This effect leads to charge collection inefficiency when the drifting charge is shifted close to the surface, where it can be trapped (Fig. 8).

Now we have to establish the relationship between the potential deviation and the systematic error component of the position resolution. Figure 9 presents the standard deviation of the drift time as a function of the defect position for different values of $\delta u$. To calculate this value we took for every drift distance the difference between the drift time in the detector with a non-linearity and the drift time in the 'ideal detector'. For a drift field of $670V/cm$ (that corresponds to a voltage drop of $8V$ between two consequent cathodes) the drift velocity is about $8\mu m/ns$. The standard deviation of the drift time, that corresponds to a systematic error of $21\mu m$ is $(21\mu m)/(8\mu m\, ns^{-1}) \simeq 3ns$. It means that in the worst case (when the defect is in the middle of the drift region) the variation $\delta u$ should not be greater than $0.1V$ (Fig. 9). It corresponds to a maximum potential deviation

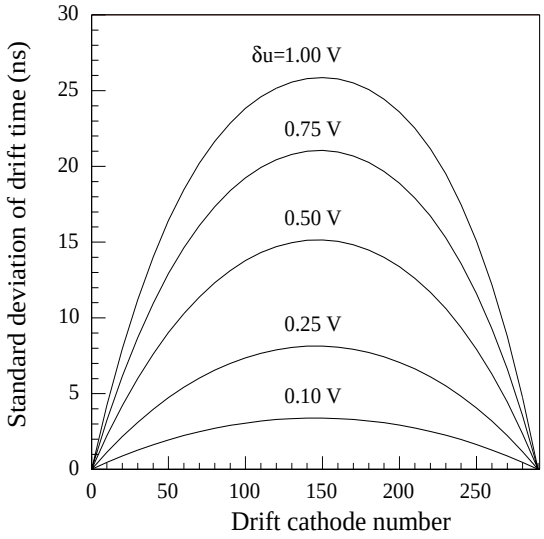


Figure 9: Standard deviation of the drift time as a function of the defect position.

$\Delta U$ of $7.0V$ (Fig. 7). From equation (4) the current generated by this defect is $600nA$.

The linearity of the potential on the divider is affected also by the hole dark current. Let's suppose that all resistors of the integrated high voltage divider have a constant value $r$ and the hole dark current is zero. In this ideal case the voltage drop $u$ between any two adjacent drift cathodes is constant and determined as $u = rI_{div}$, where $I_{div}$ is the current flowing through the cathode chain. In the real conditions there is always the hole dark current entering the drift and guard cathodes and for the drift cathode $k$ the voltage drop is $u' = r(I''_{div} + ki_{dark})$, where $i_{dark}$, supposed constant, is the hole dark current entering one cathode, while $I'_{div}$ is the divider current. In this situation

$$U_{bias} = 291rI''_{div} + ri_{dark}\sum_{k=1}^{291} k, \tag{6}$$

so

$$I''_{div} = \frac{U_{bias}}{291r} - 146i_{dark} = I_{div} - 146i_{dark} \tag{7}$$

As a result, the potential distribution is no longer horizontal, but it presents some slope (Fig. 10a). The potential on the cathode $k$ (Fig. 10b) is now described by the following equation:

$$U(k) = U_{ideal}(k) - (291 - k)r\left(146 - \frac{292 - k}{2}\right)i_{dark}. \tag{8}$$

The dark current influence on the linearity of the potential distribution was simulated for the large area prototype. Figure 11 shows the dependence of the maximum

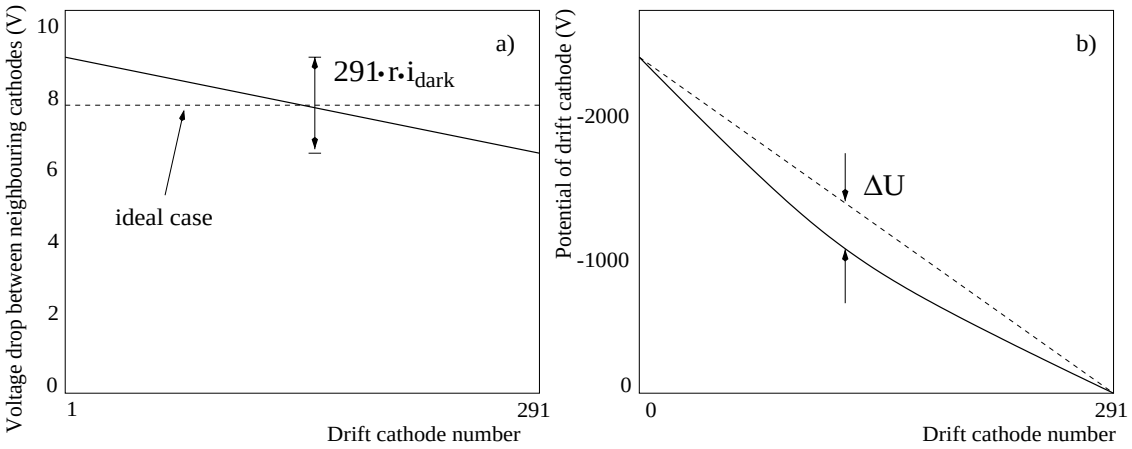


Figure 10: Effect of the dark current: on the potential drop between neighbouring drift cathodes (a), on the potential on the divider (b).

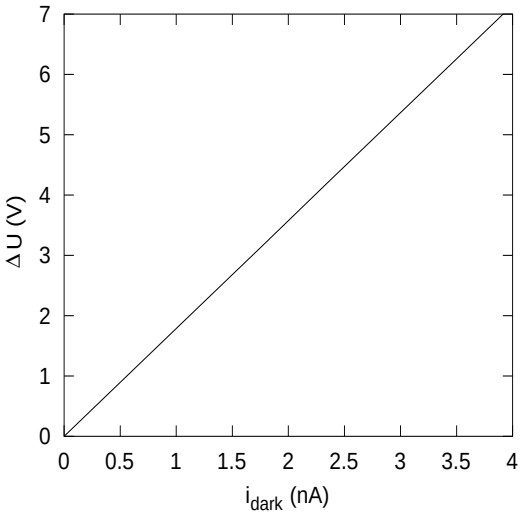


Figure 11: Maximum variation of the potential on the divider as a function of the dark current entering one drift cathode.

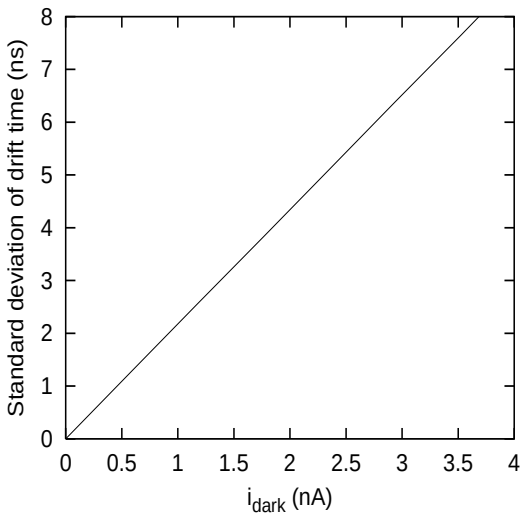


Figure 12: Standard deviation of the drift time as a function of the dark current entering one drift cathode.

deviation ($\Delta U$) of the potential distribution on the dark current that enters one drift cathode. The deviation reaches its maximum in the middle of the drift length (cathode # 145). Figure 12 gives the standard deviation of the drift time as a function of the dark current entering one drift cathode. Considering the limit, previously determined, of $3ns$ on the drift time standard deviation, from this plot we can get a value of $1.5nA$ for the maximum affordable dark current per cathode. Since the electron component of the dark current is collected by the anodes, it is useful to calculate the current per anode corresponding to $1.5nA$ per cathode. This value is given by the number of drift cathodes on both sides of

the detector multiplied by the current per cathode and divided by the number of anodes. It results in $3.5nA$.

To come to the conclusion, when we have to verify the quality of a detector there could be two cases:

- the detector is free of defects:
  we have to check whether the current per anode is within the limit of $3.5nA$,

- the detector presents a defect:
  a) we have to establish the value of the mean current per anode without considering the *hot-spot*. If it is lower than $3.5nA$ we have to verify whether the voltage step generated by the defect (Fig. 6a) is within the specifications. Figure 13 gives the maximum allowable value of $\delta u$ as a function of the dark current per anode.
  b) We have to check whether the current entering one anode is lower than $100nA$ (requirement regarding the front-end electronics).

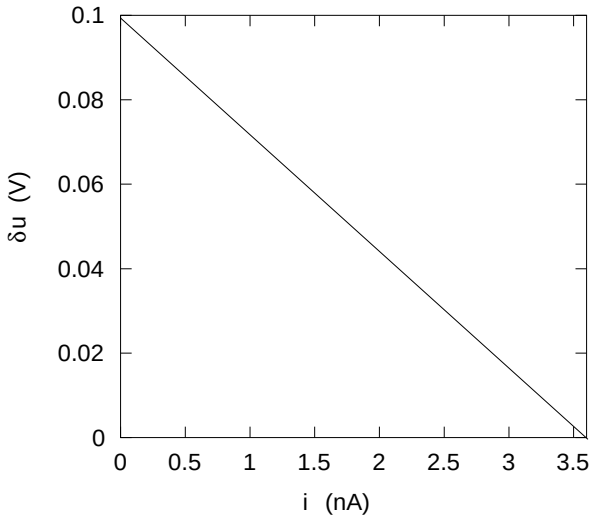


Figure 13: Maximum allowable variation $\delta u$ of the potential drop between consequent cathodes as a function of the dark current per anode.

## 4 Measurements.

In this section we analyse two detectors: one is free of defects, while the other has a number of local defects on one side. We apply the conditions determined in the previous section to verify if these SDDs are within the specifications. We also introduce a fast $(I-V)$ measurement that gives indications about the currents in the detector. Indeed, the

complexity of the SDD requires several hours to perform a full analysis using a dedicated double sided probe station. Taking into account the large number of SDDs foreseen for the ALICE ITS, it is useful to make some fast and simple preliminary measurements of $(I-V)$ characteristics in order to perform a first selection. As soon as all drift cathodes are connected together through the integrated voltage divider, it is enough to use two probes to bias the whole cathode chain. The first probe is put to one of the cathodes and the second one is put to the bulk contact. This has to be done for both $n-$ and $p-$side of the detector.

### 4.1 Defect-free detector.

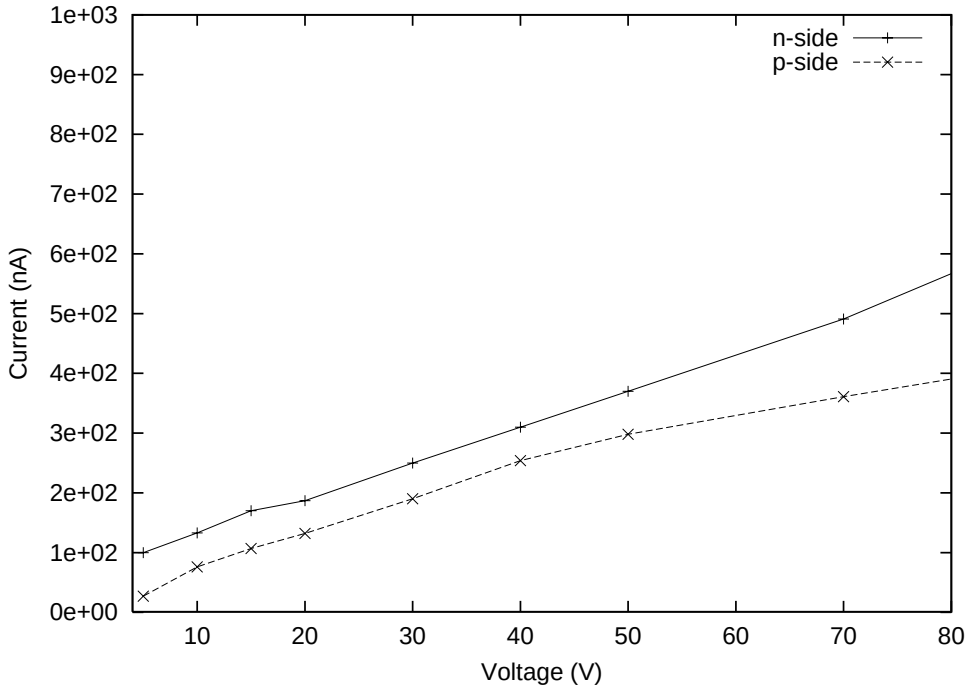


Figure 14: $(I-V)$ characteristics of the detector free of defects.

$(I-V)$ characteristics are shown in figure 14. We measured the leakage current up to a bias voltage of $-80V$, even though the working value referred to the bottom of the potential gutter is around $-30V$. One can observe a normal increase of the current due to the increment of the depleted volume and so there is no indication of local defects. The values of the current at $-30V$ for both sides are about $200nA$, so one can expect that the average current per anode will be of the order of $1nA$ in the working conditions: a value well below the limit of $3.5nA$ found in the previous section.

The detailed analysis confirmed these expectations. Figure 15 shows the distribu-

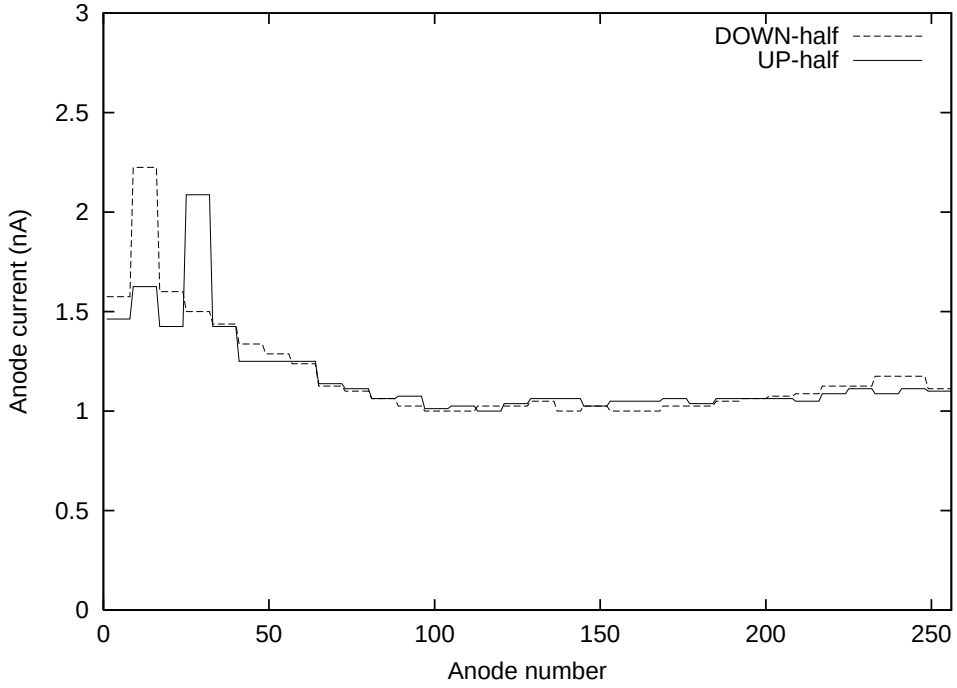


Figure 15: Distribution of the anode current.

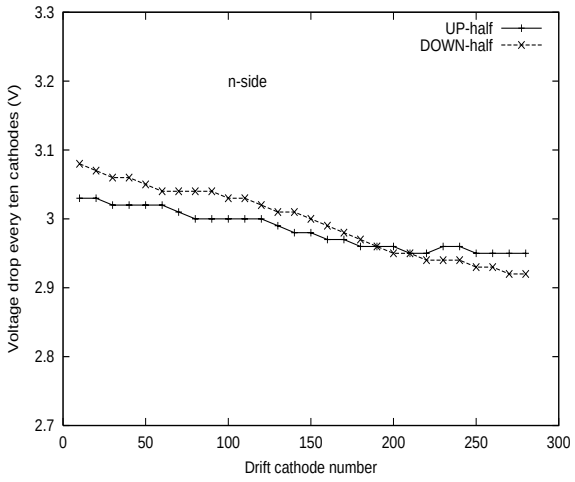


Figure 16: Voltage drop every ten drift cathodes for the $n-$side.

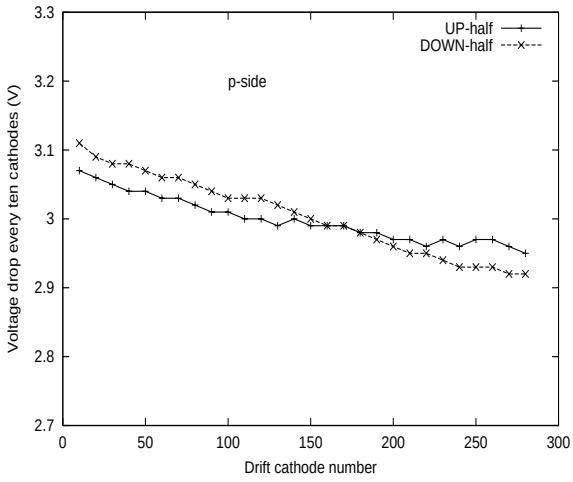


Figure 17: Voltage drop every ten drift cathodes for the $p-$side.

tion of the anode current for both halves of the detector biased at $-2400V$. The current was measured connecting together $8$ anodes at a time and the plot presents the resulting average current per anode of about $1nA$. Figures 16 and 17 present the potential drop be-

tween ten consecutive drift cathodes as a function of drift cathode number. All curves are free of steps generated by local defects. They only present the slope attributed to the dark current. From this plot it is possible to extract an average value of $0.3nA$ for the hole dark current that enters one cathode. It results in an average current per anode of $0.7nA$ which fits well the measured value. The potential distribution was measured at a bias voltage of $-100V$ because at higher voltages its linearity starts to be affected by a *punch-through* current between the guard strips (this phenomenon is not discussed in this paper because its origin does not deal with the leakage current). Anyway, figure 18, showing the total leakage current as a function of the bias voltage, proves that rising the bias voltage till

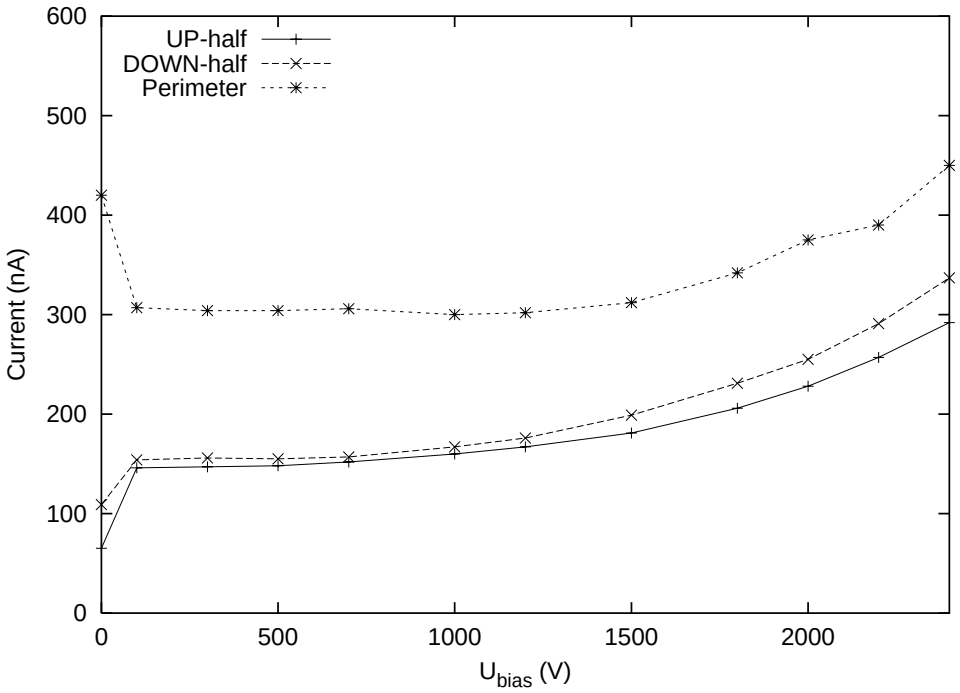


Figure 18: Leakage currents as a function of the potential on the divider.

$-2400V$ neither the slope of the curves presented in figures 16-17 becomes critical nor any local defect appears. The slight increase of the leakage current can be explained by the temperature growth of the detector bulk due the current flowing through the integrated divider.

It is possible to conclude that this detector is within the specifications.

### 4.2 Detector with local defects.

Figure 19 shows $(I-V)$ characteristics for $n-$ and $p-$side of the detector. $p-$side has a leakage current of $350nA$ at $-30V$ that gives an average current of $0.6nA$ per cathode

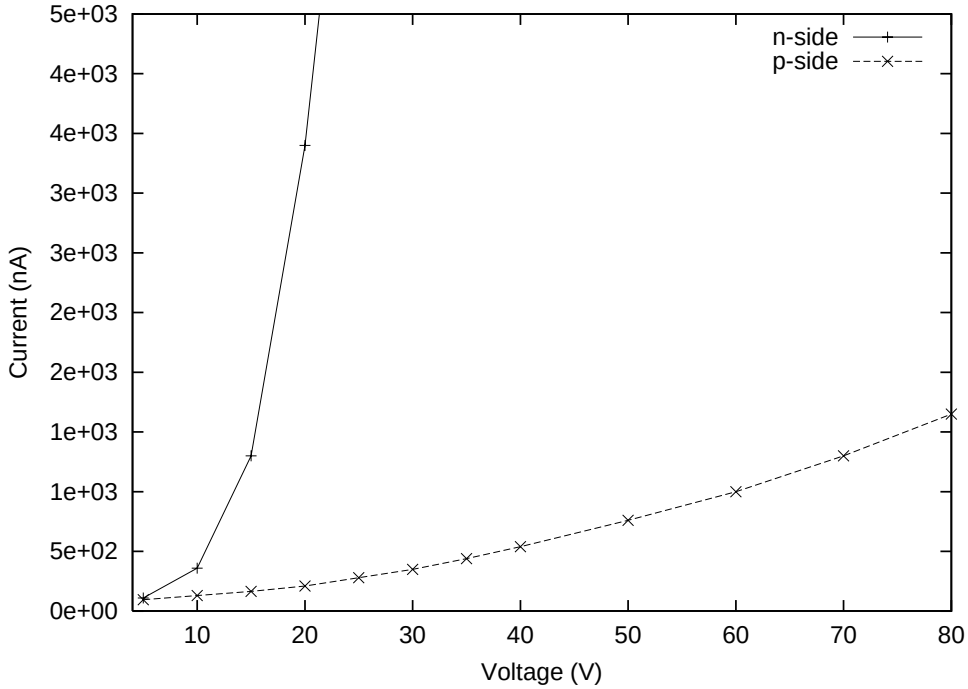


Figure 19: $(I-V)$ characteristics of the detector with defects.

and promises a good potential distribution on the divider of $p-$side. On the other hand $n-$side clearly presents serious problems even at low voltages.

The subsequent detailed analysis confirmed the conclusions of the preliminary test. Figure 20 is a plot of the anode current distribution measured on the two halves of the detector. '*Hot spots*' of the current are clearly visible and point to the presence of several local defects in the sensitive zone of the detector. Moreover there are two peaks that bring the detector out of specification, since their value is greater than $100nA$. Figures 21-22 show the potential drop between ten consecutive drift cathodes as a function of the cathode drift number. From the slope of the potential drop of the $p-$side we can get a value of $0.5nA$ for the average current per cathode which is close to the value predicted by the preliminary $(I-V)$ measurements. $n-$side distribution is marked by few steps generated by local defects. Near the cathode # 210 of one detector half there is also a pronounced peak that can be attributed to a defective resistor of the integrated divider. It is easy to verify that $n-$side is out of the requirement regarding the position resolution. In fact, the variation $\delta u$ of $1.8V/10$ that happens in the group of cathodes #100-#110 of the "UP-half" alone is enough to make this detector unusable (see the previous section).

The conclusion is that this detector is out of requirements regarding both the front-end electronics and the position resolution.

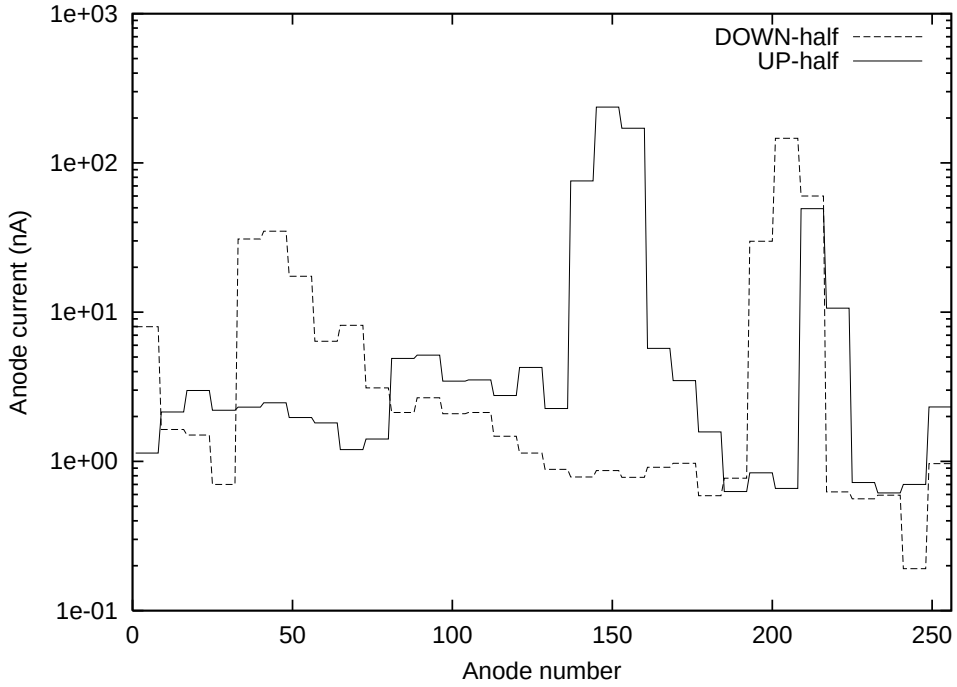


Figure 20: Distribution of the anode current.

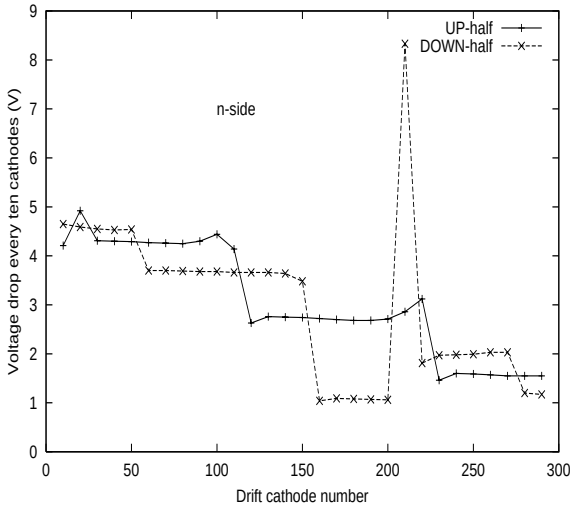


Figure 21: Voltage drop every ten drift cathodes for the $n-$side.

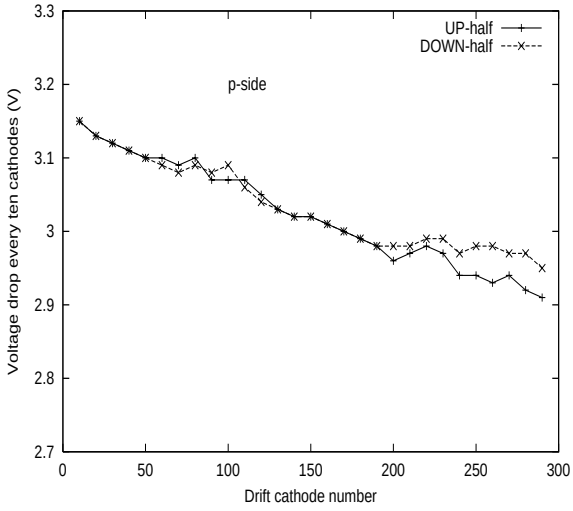


Figure 22: Voltage drop every ten drift cathodes for the $p-$side.

## 5 Acknowledgements

The authors wish to thank Valter Bonvicini, Andrea Vacchi, Richard Wheadon for the fruitful discussions, and Nicola Zampa for his help in preparing the measurement set up.

## References

[1] E. Gatti and P. Rehak, Nucl. Instr. and Meth. **A225**, 608-614 (1984).

[2] E. Gatti and P. Rehak, Nucl. Instr. and Meth. **A226**, 129-141 (1984).

[3] P. Rehak *et al*, Nucl. Instr. and Meth. **A235**, 224-234 (1985).

[4] P. Rehak *et al*, Nucl. Instr. and Meth. **A248**, 367-378 (1986).

[5] E. Gatti *et al*, Nucl. Instr. and Meth. **A253**, 393-399 (1987).

[6] Inner Tracking System, ALICE Technical Design Report, CERN/LHCC, June 1999.

[7] A.Vacchi *et al*, Nucl. Instr. and Meth. **A306**, 187 (1991).

[8] G. Gramegna *et al.*, IEEE Trans. on Nuclear Science, Vol. **42**, No. 5, October 1995.

[9] G. Gramegna *et al.*, Nucl. Instr. and Meth. **A360**, 110-112 (1995).

[10] S. Beole' *et al.*, Nucl. Instr. and Meth. **A360**, 67-70 (1995).

[11] S. Beole' *et al.*, Nucl. Instr. and Meth. **A377**, 393-396 (1996).

[12] S. Beole' *et al.*, Il Nuovo Cimento, Vol. **109** A, N. 9, September 1996.

[13] R. Bellwied *et al.*, Nucl. Instr. and Meth. **A400**, 279 (1997).

[14] A. Rashevsky *et al.*, Nucl. Instr. and Meth. **A409**, 210-215 (1998).

[15] E. Gatti *et al.*, Nucl. Instr. and Meth. **A295**, 489 (1990).

[16] V. Bonvicini *et al.*, Il Nuovo Cimento, Vol. **112A**, N. 1-2, January-February 1999.

[17] V.Bonvicini *et al.*, paper presented at the 8th European Symposium on Semiconductor Detectors, Schloss Elmau, Germany, June 14-17, 1998, to be published in Nucl. Instr. and Meth. A.